Journal of Applied Polymer Science

# Viscoelastic properties of polyaniline-emeraldine base nanostructured films: Experimental results and molecular dynamics simulations

**Alireza Bahramian**
Department of Chemical Engineering, Hamedan University of Technology, Hamedan 65155, Iran
Correspondence to: A. Bahramian (E-mail: bahramian@aut.ac.ir)

**ABSTRACT:** Comprehensive exploration of the viscoelastic properties of polyaniline–emeraldine base (PANI–EB) nanostructured films is presented from two viewpoints of experimental study associated with dynamic mechanical thermal analysis and thermogravimetric measurements and of computational simulations by molecular dynamics (MD) approach. The results are expressed in storage and loss modulus components ($E'$ and $E''$). The role of drying temperature, time, and residual solvent content were studied on the $E'$ and $E''$ of prepared PANI–EB films. Using the principle of time–temperature superposition, $E'$ and $E''$ at different temperatures and frequencies can be plotted on master curves. The relationship between the modulus components with the solvation level of PANI–EB film is also studied. MD simulation is applied to study the viscoelasticity of simulated PANI structures with different monomeric aniline chains. The temperature dependence of viscoelastic properties provides good information for fractional free volume, cavity size distribution, and activation energy of PANI structures. Simulation outcomes provide a fairly good compatibility with the experimental results. © 2014 Wiley Periodicals, Inc. J. Appl. Polym. Sci. **2015**, *132*, 41858.

**KEYWORDS:** nanostructured polymers; viscosity and viscoelasticity; theory and modeling

Received 7 October 2014; accepted 2 December 2014
**DOI: 10.1002/app.41858**

## INTRODUCTION

Conductive polymer thin films are widely used in many technological applications including microelectronics,[1–3] optics,[4–6] energy storage,[7,8] mechanical actuators,[9] and biomedical devices.[10] The viability of mentioned applications and performance of prepared optoelectronic devices depend on the viscoelastic properties of the polymer thin films that determine their process ability and mechanical integrity. For example, previous researches have shown that the surface viscoelasticity modulate of the polymer dielectric layer can change the morphology of pentacene; thus, it can adapt the transistor performance.[11–13]

In determining the viscoelastic properties, it is important that one assess the tendency of polymer film to absorb solvent and moisture. This property can be disturbing during the evaluation of mechanical properties if no specific cautions are taken. In the case of polymer films, it has been known that charge transport, on which virtually all applications rely, is promoted by a high level of solvent content as this declines the resistance to ion motion in the polymer film. The underlying requirement to answer this defect is an independent manipulation of mechanical and electronic properties of film. In the polymer films, the network structure surrounds the organic solvent from the surface tensional force and prevents it from passing from the network structure. In other words, residual solvent content remains inside the film structure, and the polymer network acts as a container that can hold a considerable amount of solvent and necessarily result in film softening. This phenomenon may be nearly related to those believed to be strongly operative in nanostructured polymer films where polymer reach to nanoscale dimensions (typically >100 nm in thickness) appears to severely affect the glass transition temperature $T_g$. Since the early studies on the glass transition behavior of nanoconfined polymer films by Keddie *et al.*,[14,15] there has been growing evidence that the physical and mechanical properties of polymer chains are limited at the nanoscale dimension, including the $T_g$, and viscoelastic properties vary considerably from the bulk properties of same polymer.

Polyaniline (PANI) is one of the most interesting conductive polymers because of its solubility, process ability, and environmental stability. In addition, the PANI is a high-performance polymeric film because of its crystallinity and structural rigidity.[16,17] Among the different oxidation states of PANI, the emeraldine base (EB) form, which is composed of half oxidized units and half reduced ones, can be doped into a conducting polymer. Most of the previous works have focused on the electron

Additional Supporting Information may be found in the online version of this article.

and ion transport in the PANI–EB films through study on the electrical conductivity,[16,18,19] crystalline structure,[17,20] and thermal properties[21–23]; however, the controlling dynamics and viscoelasticity of polymer has been less paid attention. Despite the desirability of high electronic conductivity, study on the viscoelastic properties of the PANI–EB films as the basis of technological applications is critical. In addition, they are effective factors in film longevity or in controlling device performance. In the first case, performance is dictated by the stiffness of the PANI film, parameterized through the storage modulus, $E'$, whereas in the latter case, performance is dictated by the viscosity of the PANI structure, parameterized through the loss modulus, $E''$.

In the PANI thin films, although $T_g$ is fairly insensitive to the thickness of film, the heat treatment can exert as an effective parameter on the traction rate of the polymer crosslinking, and the content of residual solvent within the film affects the surface viscoelasticity modulates. In the past few years, PANI/solvent systems have been studied, which yield highly conducting film when the solvent is removed and have the conductivities in the range $10^{-6}$ to $10^{2}$ S/cm.[24–26] Therefore, it can be shown that there is a direct relationship between the content of residual solvent and the conductivity and rheological behavior of the PANI film. For example, Garai *et al.*[27] investigated the viscoelastic and conductivity properties of thermoreversible PANI–dinonylnaphthalene sulfonic acid system that was solved in *m*-cresol as an organic solvent. They found that an increase in solvent concentration at the same frequency measurement leads to an increase of approximately three and five orders in the conductivity and viscoelastic module of the PANI film, respectively. They also suggested that the significant increase in the aforementioned properties is resulted from the formation of crosslinked structures between the PANI chains in the *m*-cresol.

The measurement of the viscoelastic properties of polymer thin films can be performed using various techniques such as dewetting,[28] nanobubble inflation,[29] electrohydrodynamic instability,[30] X-ray photon correlation spectroscopy,[31] dynamic mechanical thermal analysis (DMTA), and acoustic wave method.[32–35] DMTA measurement and parameterization in terms of shear modulus, $E = E' + jE''$ [$j = \sqrt{(-1)}$ represents the phase relationship], can be applied to determine the viscoelastic properties of polymer thin film under heat treatment and description of transition from the glassy to rubbery state in this process.

Commonly, proof-of-concept for the viscoelastic properties of the PANI–EB thin film is established and favorable results are obtained. However, the technological instrumentation is restricted by the following points: (1) the inability to measure the temperature-dependent modulus and viscosity, (2) the lack of applicability to small-length scales because of their complexity, (3) crosslinking phenomena between PANI chains especially in the rubbery state, and (4) polymer durability or device longevity; in many cases, these limitations are indistinguishably interconnected. Thus, it is desirable to develop computational methods that overcome these limitations. Molecular dynamics (MD) simulation defeat the limitations of traditional empirical approaches and showed wonderful potential for studying the structural and physical properties of the polymer thin films.[36,37]

In this study, an integrated approach of experimental results and MD simulations is used to explore the dynamic and viscoelastic properties of the PANI–EB nanostructured film. Experimentally, viscoelastic properties of prepared crosslinked PANI films exposed to irregular nanofibers are studied based on the different parameters such as drying temperature and time, residual solvent content, surface structure, and morphology of film. Thermogravimetric analysis (TGA) and DMTA measurements were carried out to determine the thermal properties and dynamical viscoelastic parameters of the PANI–EB film, such as $E'$ and $E''$ as functions of dynamic frequency and temperature. The relationship between the $E$ with the solvation level of PANI–EB film is investigated. Subsequently, modulus components were tabulated from experimental data, and master curves were generated at a reference temperature using the principle of time–temperature superposition (TTS). Computationally, MD simulation is applied to study the dynamic and viscoelastic properties of simulated PANI structures consisting of 30, 40, and 50 monomeric aniline chains. The temperature dependence of viscoelastic properties can provide information concerned with free volume fraction, cavity size distribution (CSD), and activation energy of generated PANI structures. The MD simulation outcomes provide a fairly good compatibility with the experimental results.

## EXPERIMENTAL

### Chemicals

Aniline (99.5%, ACS reagent grade), ammonium peroxydisulfate [$(NH4)_2S_2O_8$, 98% ACS reagent grade], 1-methyl-2-pyrrolidinone (NMP, HPLC grade), hydrochloric acid (HCl, 37.43% ACS reagent grade), and ethanol (99.9%) are used in this study. All chemicals were purchased from Sigma-Aldrich.

### Polymerization Procedure

PANI was prepared by the chemical reaction of aniline using $(NH4)_2S_2O_8$. At first, aniline was dissolved in a 0.25*M* $(NH4)_2S_2O_8$ as an oxidant agent and 0.5*M* HCl solution as a catalytic agent by continuous mixing at room temperature for 12 h to obtain 0.55*M* aniline. The prepared solution was cooled down to $-5$°C to obtain PANI–EB precipitate. The precipitate was filtered, and the obtained cake was washed at first with pure ethanol and then with deionized water for several times. The wet precipitate was dried at 323 K under vacuum conditions for 3 h. The obtained green PANI–EB powder was added to 100 mL of NMP as a solvent under mixing for 2 h at room temperature to make a solution with 15 wt % PANI. Finally, a homogenous solution with a brownish green color was obtained.

### Preparation of Films

The PANI–EB thin films were obtained by the immersion of ultrasonically well-cleaned soda lime glass as a substrate into homogenous solution, which was prepared as in the previous section, using dip-coating method.[38] The withdrawal speed of the substrates is controlled to $1.0 \times 10^{-3}$ m/s. The thickness of the thin films was adjusted by repeating the cycle from dipping process. Then, a heat treatment was applied, when each wet film was dried in the oven under vacuum conditions at drying temperatures ranging from 298 to 418 K and drying time from 5 to 24 h. However, the NMP solvent (b.p. 475–477 K) could

not be completely removed from the films during the heat treatment. The samples were then cooled to ambient temperature before the analysis and experimental measurements. Finally, to remove the solvent effect on the viscoelastic properties of the film, NMP-free PANI–EB film was made by repeating doping (0.5*M* HCl) and dedoping (0.25*M* $NH_4OH$) processes for several times.

### Analysis and Measurement

The thickness of PANI–EB nanostructured films were determined using ZeScope optical profilometer. The surface structure of the PANI–EB nanostructured films was observed on a Cam Scan MV2300 (SEM) at an accelerating voltage of 10 kV. The surface morphology of the PANI–EB nanostructured films was observed on a TEM (Model: EM 900; Zeiss). TGA of the PANI–EB films was carried out using a Perkin-Elmer (Model Pyris 1) thermogravimetric analyzer at a heating rate of 10°C/min in flowing high-purity $N_2$ gas (15 mL/min). DMTA measurements were carried out on an RSA III (TA Instruments) dynamic mechanical thermal analyzer. The dynamic viscoelastic parameters of the PANI–EB thin film, such as shear storage module and loss module as functions of dynamic frequency ($\omega$) and temperature ($T$), were determined over a temperature range from 298 to 418 K at a heating rate of 2°C/min. The measurements were performed at 0.8 V as typical AC applied voltage in the frequency range from 10 to 200 MHz in tension mode of DMTA. Each measurement was repeated for three times, and the corresponding averages were calculated for the determination of storage modulus and loss modulus.

## MOLECULAR DYNAMICS SIMULATION

MD simulations were carried out through the discover module using the condensed-phase optimized molecular potentials for atomistic simulation studies (COMPASS) force field. In this force field, the bonded terms are originated from the Hartree-Fock model,[39] whereas the nonbonded terms and their related force field were derived from the Coulomb and van der Waals forces.

### Molecular Models of the Undoped PANI

The simulated PANI cell is constructed by adding atoms one at a time in a stepwise manner. A self-avoiding walk algorithm presented by Theodorou and Suter[40] was used to generate the undoped PANI. The molecular model of the PANI constructed for MD simulation incorporates the interactions arising from bond stretching, changes in the torsional forces, bond angle, and nonbonding interactions. These interactions appear as energy terms in the potential function derived from the COMPASS force field expressed by the following equation:[7,36,41–44]

$$E(r^N) = \sum^{N\,\text{bonds}} E_{\text{bond}} + \sum^{N\,\text{pairs}} E_{\text{nonbond}} + \sum^{N\,\text{angles}} E_{\text{angle}} + \sum^{N\,\text{torsions}} E_{\text{torsion}}, \quad (1)$$

where $E_{\text{bond}}$ represents the energy associated with bond stretching, $E_{\text{nonbond}}$ represents the contributions to the total energy of the nonbonded interactions arising from the electrostatic interactions between pairs of atoms separated by two or more intervening atoms and the van der Waals interactions, $E_{\text{angle}}$ is the energy associated with the changes in the bonds' angles, and $E_{\text{torsion}}$ denotes the contribution of the torsional forces. The detailed energy terms in the potential function and their constants can be found in Supporting Information Tables S1 and S2 and eqs. (S1)–(S7).

### Molecular Models of the PANI Doped by Cl

At first, a repeating unit of the PANI structure was constructed. Second, the double bonds between carbon and nitrogen atoms were broken at the linking of the diimine chains. Third, the chlorine and hydrogen atoms were linked to the nitrogen atoms through the single bonds at various positions. The polymer was then constructed using monomers by breaking the chlorine and the nitrogen bonds to generate the PANI–Cl structure. Depending on the monomeric aniline chains (30, 40, and 50), chlorine atoms were incorporated into the polymer chain. Finally, each subunit in the chain having a Cl atom added to polymer to arrive a fully doped PANI structure and obtained configuration of polymer was neutralized.[36,45,46] The simulated cells of the PANI doped by Cl at different temperatures are shown in Supporting Information Figure S1.

### Simulation Details

MD simulations were carried out on the constructed PANI–Cl structure consisting of 30, 40, and 50 monomeric aniline units based on the energy minimization method. Periodic boundary conditions (BCs) were used to check the surface effects and account for the nonbonded interactions.[47] Periodic BCs considerably decrease the computational time through the selection of proper calculation procedures such as cutoff distance, which is smaller than the intermolecular one. The temperature was checked by coupling the simulated structure to a heat bath. The chain is modeled as a linear string of beads linked by springs. The van der Waals force between all monomer pairs were considered to be modeled by the 9-6 type of Lennard-Jones potential function.[36,48,49]

A cubic simulation cell was used in which the bonds forming the PANI's structure were positioned in random directions. According to the applied temperature, the length of the simulation cell's side fluctuated from 34 Å to about 42 Å. The density of the constructed PANI was set at 0.15 g/cm$^3$ at the start of the energy minimization method to prevent spearing of repeating chains of the packing algorithm. To increase the density, the simulation cell was compressed at a pressure in the range of 0.7–1.1 GPa. The MD simulations were performed in the isothermal–isobaric (*NPT*) ensemble to increase the polymer density and make it as close as possible to the experimental value of 1.245 g/cm$^3$ at 298 K.[50] Subsequently, MD simulations were performed in the canonical (*NVT*) ensemble with an initial temperature of 298 K. The minimum value of the ambient temperature ($T = 298$ K) was selected to investigate the simulation outcomes in computationally feasible simulation times. The simulations were carried out at temperatures ranging from 298 to 418 K in 10 K intervals. Finally, the simulated PANI structure was steadily cooled down to the initial temperature in steps of 10 K. The temperature was adjusted by the algorithm of Nosé-Hoover thermostat, whereas the pressure was studied by the Andersen algorithm.[51,52] Depending on the stability of the

system with monomeric aniline chains of 30, 40, and 50, the timescales changed from 5 to 7 ns and then 10 ns, respectively. The time step of 0.001 ns is selected in all simulations to obtain stabilized molecular structure of PANI. Based on the monomeric aniline chains used in the mentioned system, the total simulation time required for a constructed PANI–Cl system at the equilibrium state was varied from about 72 to 96 h by a PC with a 3.2-GHz Pentium 4 CPU.

### Determination of Cavity Size Distribution

During the construction of the simulated PANI structure, it is possible to create some cavities and voids because of the interatomic forces. The CSD examines the effect of free volume fraction on the diffusion coefficients of gases and liquids in materials. It is noteworthy that the position-annihilation lifetime spectroscopy, as an experimental technique, is an expensive method for the determination of the CSD of a polymer film. Therefore, MD simulation can be used as an alternative technique for the determination of the CSD. A cavity energetic sizing algorithm (CESA),[47] which is a combination of MD and Monte Carlo simulations, was used to each of the simulated PANI structures for the calculation of CSD. In CESA method, a spherical volume is applied to describe a cavity with a distinct center, which represents a lowest value in a repulsive particle energy field. The average cavity size $\langle x \rangle$ is expressed as follows:

$$\langle x \rangle = \frac{\int_0^\infty x^3 P(v)\,dx}{\int_0^\infty x^2 P(v)\,dx}, \tag{2}$$

where $x$ is the cavity size, and $P(v)$ is the volume distribution, which was calculated by CESA algorithm.

### Calculation of Viscoelastic Properties

The shear stress modulus $E(t)$ for each PANI–EB chain was calculated by the time autocorrelation function (TACF) of stress tensor.[53,54]

$$E_{xy}(t) = \frac{V}{k_B T}\langle P_{xy}(t) - P_{xy}(0)\rangle, \tag{3}$$

where $P_{xy}(t)$ is an instantaneous of the off-diagonal component of the stress tensor at time $t$ in the plane $(xy)$ vertical to the direction of the cylinder positioned along the longitudinal direction, $V$ is the volume of the system, and the brackets denote an average over the whole trajectory and all components of the stress tensor. The shear modulus of the PANI–EB film was calculated by the averaging of three off-diagonal components of the symmetric stress tensor.

Supposing that dynamics of a polymer structure can be expressed as a superposition of independent normal modes, the shear modulus $E(t)$ of a polymer chains can be represented as follows:[53]

$$E(t) = c_p k_B T \sum_{p=1}^{N_{seg}-1} \frac{\langle X_p(t) - X_p(0)\rangle^2}{\langle X_p(0).X_p(0)\rangle^2}, \tag{4}$$

where $c_p$ is the polymer chains for each unit volume, $N_{seg}$ is the statistical segments in the polymer chain, and $X_p(t)$ is the $p$th normal mode of polymer chain, which is defined as follows:[51]

$$X_p(t) = \sqrt{\frac{2}{N}} \sum_{n=1}^{N} cos\left(\frac{n - 1/2(p\pi)}{N}\right) R_n(t), \tag{5}$$

where $p$ is the mode index $(1 \le p \le N)$ and $R_n$ is the coordinates of the polymer chain in the Cartesian direction of the $n$th bead. Equation (4) is used based on the assumption of homogenous PANI dynamics, which means that all PANI chains relax equally:[51]

$$\frac{\langle X_p(t).X_p(0)\rangle^2}{\langle X_p(0).X_p(0)\rangle^2} = \frac{\langle X_p(t).X_p(0)^2\rangle}{\langle X_p(0).X_p(0)^2\rangle}. \tag{6}$$

The TACF is obtained from the Rouse model as follows:[55,56]

$$\frac{\langle X_p(t).X_p(0)\rangle}{\langle X_p(0).X_p(0)\rangle} = \exp\left[-\left(t/\tau_p\right)^\beta\right], \tag{7}$$

where $\tau_p$ is the characteristic relaxation time for each normal mode and $\beta$ is a stretching parameter. The values of $\beta$ can be varied from 0.95 for $P = 1$ (chain relaxation) to about 0.75 for $P = 13$.[57]

Returning to the dynamical behavior near the glass transition region, it can be mentioned that a special characteristic feature is the ubiquity according to the Kohlrausch–Williams–Watts (KWW) equation:[58]

$$P(\phi(t)) = \exp\left(-(t/\tau_{KWW})^\beta\right), \tag{8}$$

where $\tau_{KWW}$is a characteristic relaxation time used as a stretching parameter.

## RESULTS AND DISCUSSION

Viscoelastic behavior of the PANI–EB films are investigated from two viewpoints: an experimental study associated with DMTA and TGA analysis and dynamical simulations using MD approach. The results of each section are presented.

### Experimental Results

At first, the surface structure and morphology of the films were studied to ensure whether the prepared films at different temperatures are composed of nanostructures, which are defined as nanostructured films. In the next step, the viscoelastic properties of prepared films were investigated.

Figure 1 represents the SEM micrographs of PANI–EB nanostructured films at drying temperature of 298 K (a) and 398 K (b), respectively. A coil-like conformation with a persistence length much larger than the conjugation length is observed in similar linear conjugated polymers. As can be seen from both figures, the surface morphology of the PANI–EB film is not enough dense, and some irregular nanofibers which are exposed to the hollow structures can be seen. However, it can be found that at $T = 398$ K, so-called rubbery state, the high evaporation rate of NMP trapped in the structure causing the formation of significant small "holes" in the surface of PANI–EB film [Figure 1(b)].This existence of voids suggested incomplete adhesion or wetting in the PANI–EB film during heating process. The SEM image analysis is shown in Figure 2, as indicated by the histograms given in Figure 2(a) ($T = 298$ K) and Figure 2(b) ($T = 398$ K). It can be found that the number–average diameter of voids are 183 nm (with diameter distribution ranged from 35

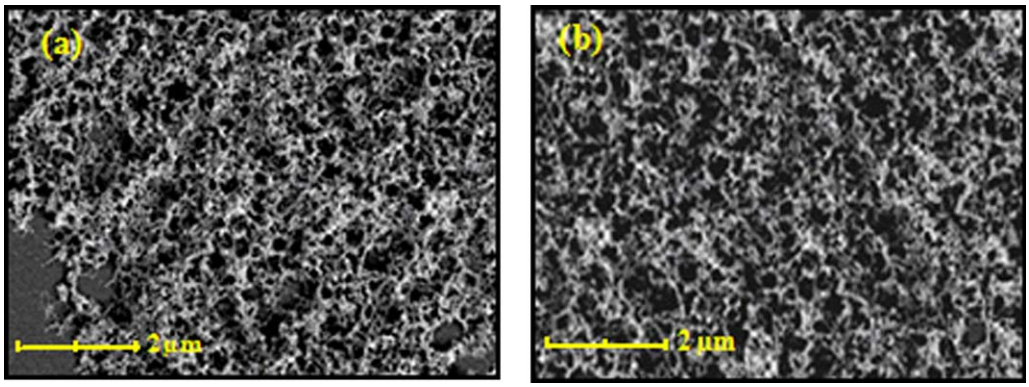


**Figure 1.** SEM images of PANI–EB nanostructured film prepared at temperatures of 298 K (a) and 398 K (b). [Color figure can be viewed in the online issue, which is available at wileyonlinelibrary.com.]

to 400 nm) and 209 nm (with diameter distribution ranged from 60 to 420 nm), respectively. It can be noted that the increase in drying temperature from 298 [Figure 1(a)] to 398 K [Figure 1(b)] appears to favor the coalescing of nanofibers, thereby yielding a less homogeneous surface morphology. The mean thickness of PANI–EB films was determined to $460 \pm 15$ nm using ZeScope optical profilometer.

Figure 3 represents the TEM micrographs of PANI–EB nanostructured films at drying temperature of 298 K [Figure 3(a)] and 398 K [Figure 3(b)], respectively. TEM micrograph shows that the PANI–EB structure consists of high aspect ratio of physical crosslinked nanofibers, having diameters between 28 and 82 nm [Figure 3(a,b)] and lengths up to several hundred nanometers. It can be seen that the increase of drying temperature from 298 to 398 K led to an increase in the diameter of nanofibers from 28–59 nm range [Figure 3(a)] to 33–82 nm range [Figure 3(b)], respectively.

The dependency of the viscoelastic properties of the PANI–EB films on various factors such as drying time, residual solvent content, and temperature are separately investigated in the following sections.

**Role of Temperature.** The variations of the log $E'$ and log $E''$ as a function of temperature for the PANI–EB nanostructured film are shown in Figure 4(a,b), respectively. The measurements were performed at a constant heating rate of 2°C/min in a nitrogen atmosphere under a frequency of 110 MHz. It can be seen that the $E'$ decreased by three orders of magnitude from the values of about 5.5 (±0.2) GPa to 3.5 (±0.2) MPa in the temperature range of about 350–410 K [Figure 2(a)], which quantifies film softening with heating. However, in the same temperature range, the $E''$ increases and reaches a peak value that can be named the glass transition region which includes $T_g$ [Figure 4(a)]. The value of $T_g$ for PANI film is reported to be 378 K.[37] The cooperative motion of segments takes place in the glass transition region. In the extensively dried PANI films ($\approx T \geq 370$ K), the NMP solvent-induced molecular ordering is no longer possible, which leads to significant decrease in the $E'$.

The typical results of $E'$ and $E''$ of PANI–EB films dried at selected temperatures under a constant frequency of 110 MHz are given in Table I. According to this table, the following points should be noted: (1) In the $T \leq T_g$ range, $E'$ decreases

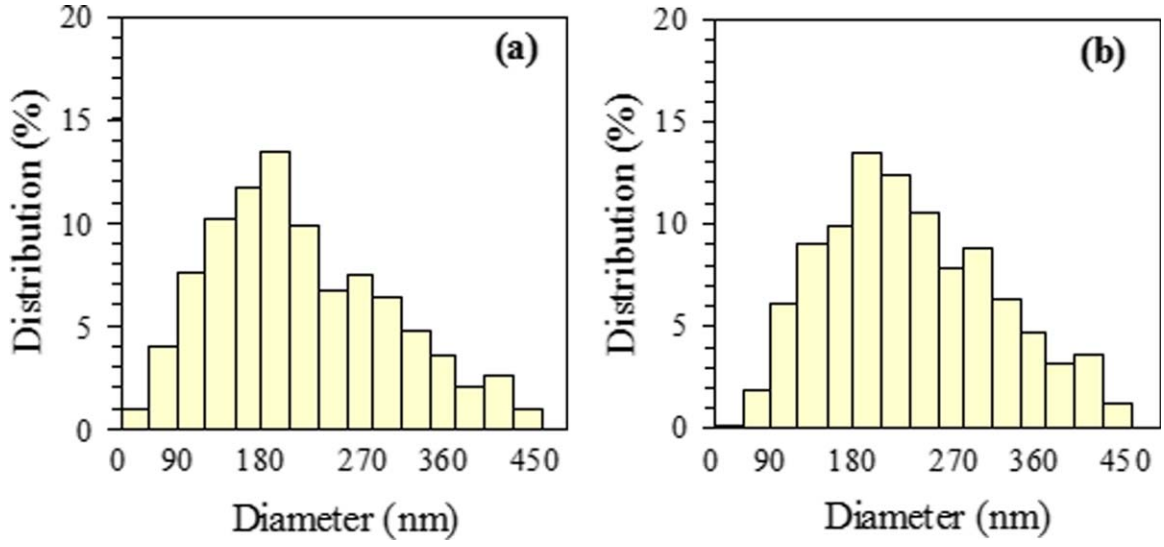


**Figure 2.** SEM image analysis of PANI–EB nanostructured film prepared at temperatures of 298 K (a) and 398 K (b). [Color figure can be viewed in the online issue, which is available at wileyonlinelibrary.com.]

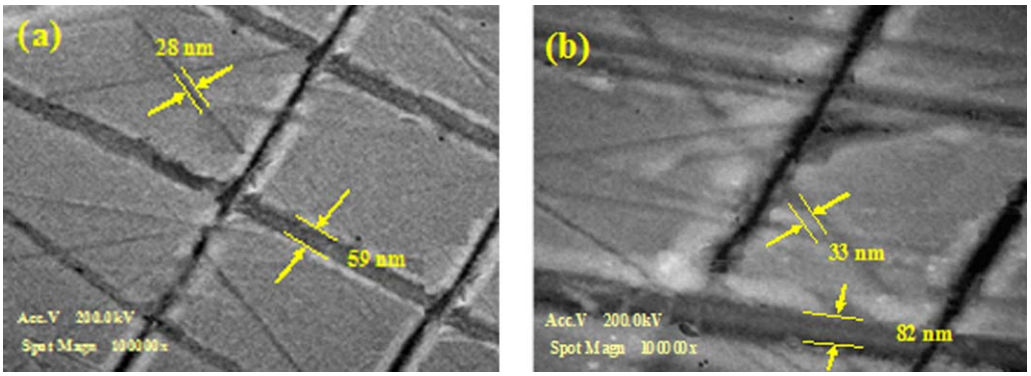


**Figure 3.** TEM images of PANI–EB nanostructured film prepared at temperatures of 298 K (a) and 398 K (b). [Color figure can be viewed in the online issue, which is available at wileyonlinelibrary.com.]

with the increase of drying temperature, so as to reach 378 K which corresponds to $T_g$ of PANI–EB film. The decrease of $E'$ showed that the plasticizing effect of NMP is more significant than both intrachain stiffening effects and interchain electrostatic interactions. (2) In the $T > T_g$ range, $E'$ decreases with the increase of drying temperature. (3) There is no linear relationship between the values of $E''$ and drying temperature. However, it can be seen that the values of $E''$ in the temperature higher than $T_g$ are smaller than the ones when $T \leq T_g$. In addition, the maximum value of $E''$ (460 MPa) is obtained at $T_g$ of PANI film.

The combined effects of temperature and frequency (timescale, $\omega\tau$) are examined by the principle of TTS.[32,34,45,59] This approach was developed for the determination of viscoelastic properties of bulk polymer thin films. The procedure of TTS is to reach shear modulus data, that is, $E(\omega,T)$, and then to combine different temperatures and timescales on a logarithmic frequency scale to generate a master curve. The second is attained using shifting curves under isothermal condition based on a reference temperature of $T_0$ chosen arbitrary; therefore, they superimpose at points of same gradient.[34,59] In the case of each isothermal data, shift factor ($\alpha_T$) is needed to obtain superposition. One of the limitations is that the shift factors should be equal for $E'(\omega,T)$ and $E''(\omega,T)$. The functional dependence of $\alpha_T$ on physical parameters shows the structural and dynamical properties of polymer.

Shear modulus components [$E'(\omega,T)$ and $E''(\omega,T)$] of PANI–EB thin film presented in log–log scale plots are shown in Figure 5. As showed in this figure, the domain of applied frequency is important in the determination of modulus components. It can be clearly seen that in the temperature ranges of 298–418 K, the change of one order of magnitude in frequency resulted in the change of $E'$ by two to three orders of magnitude. Thus, the dispersion with temperature is easier to see at high frequency. From Figure 5, several important notes can be made. (1) All slopes of log $E'$ as a function of log $f$ for PANI–EB film heated at 378 and 418 K were close to value of 2 (i.e., 1.96 and 1.96 for PANI–EB film dried at 378 and 418 K, respectively), which suggests the initial formation of a crosslinked network. It should be mentioned that the value of 2 comes from the film that starts initially as a liquid-like material.[60] (2) The temperature effect on the shear modulus component values at given frequency is not more than one order of magnitude and usually much small. (3) The $E'$ values were slightly larger than $E''$ over the whole frequency range as shown in Figure 5. (4) The increase of $E'$ with the increase of temperature from 298 to 418 K might reflect crosslinking reactions. (5) The tendency to softer films (lower $E'$) at higher temperature (418 K) is in

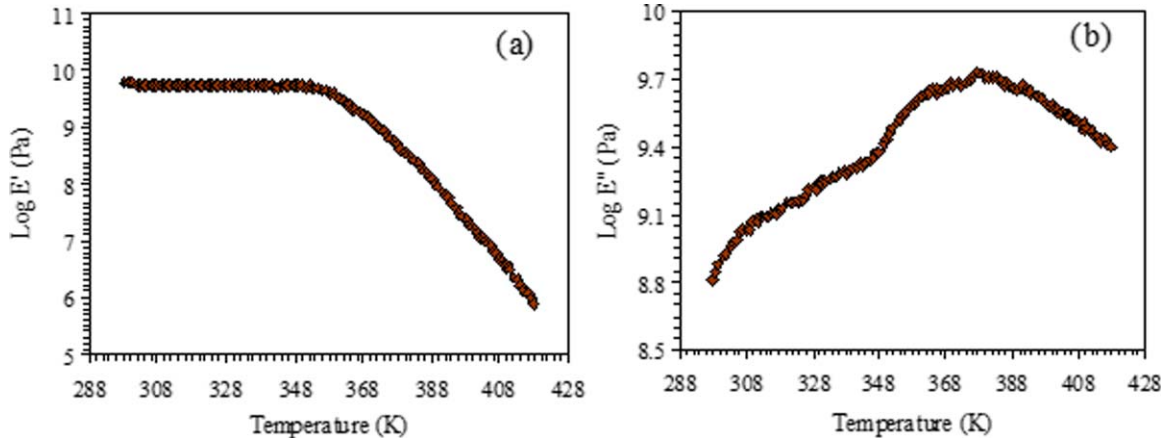


**Figure 4.** $Log_{10}$ of storage (a) and loss (b) modulus as a function of temperature for the PANI–EB film measured at a constant heating rate of 2°C/min in a $N_2$ atmosphere under a frequency of 110 MHz. [Color figure can be viewed in the online issue, which is available at wileyonlinelibrary.com.]

**Table I.** Typical Results of $E'$ and $E''$ of PANI–EB Films Dried at Selected Temperatures Measured at a Constant Heating Rate of 2°C/min in a $N_2$ atmosphere Under a Frequency of 110 MHz

| | Drying temperature (K) | | | | | |
|---|---|---|---|---|---|---|
| Parameter | 298 | 318 | 348 | 378 | 398 | 418 |
| $E'$ (MPa) | 3143 | 2900 | 2544 | 2133 | 779 | 531 |
| $E''$ (MPa) | 330 | 304 | 234 | 460 | 121 | 152 |

accordance with the idea of a shift in the direction of faster relaxation (shorter $\tau$) as mentioned in the literature.[34]

The application of appropriate shift factors to the data in Figure 5, with $T_0 = 298$ K selected as the arbitrary reference temperature, yields the master curve for PANI–EB film shown in Figure 6. Low scattering of the data (i.e., by an order of approx. 1–2) as shown in Figure 6 suggests the accuracy of the TTS applied in this study. The magnitudes of the shift factors (above unity when $T < T_0$ and below unity when $T > T_0$) result in an advantage of high-temperature data (418 K) to the left of the curves (low $E'$) and of low-temperature data (298 K) to the right of the curves (high $E'$).

A commonly used equation for the estimation of the shift factor is proposed by Arrhenius. When $T < T_g$, this model describes the relationship between the shift factor of master curve and the $T_0$ as follows:[61]

$$\log \alpha_T = \frac{E_a}{R(T - T_0)}, \quad (9)$$

where $E_a$ is the activation energy associated with the relaxation, $R$ is the gas universal constant, and $T$ is the measured temperature. The variation of shift factor, $\log \alpha_T$, as a function of $T - T_0$ for PANI–EB structure obtained by Arrhenius equation at temperatures ranging from 298 to 418 K is shown in Figure 7. The slope of this figure corresponds to the $-E_a/R$. According to Figure 7, the activation energy for degradation of PANI was found to be 20.3 kJ/mol. This result is close to the ones calculated from the data reported in the literature for degradation of PANI ($E_a \approx 21.7$–$27.5$ kJ/mol).[32,62]

**Role of Residual Solvent Content.** The NMP solvent acts as a plasticizer, softening the PANI–EB film and lubricating the movement of PANI chains past each other. The change in the content of residual solvent might be expected to result in appreciable changes in film stiffness. It is worth noting at this point that NMP can be present in two forms, simplistically referred to as "free" and "bound." There is an exchange between these two forms, however, at any instant; the solvent in each of the two forms plays a different role. "Free" NMP solvent is present to satisfy the volume and activity constraints such as activity coefficient. "Bound" NMP solvent is retained in the PANI–EB film; however, it may have a structural role that influences the viscoelastic behavior of PANI–EB thin film.

The thermogravimetric curve of PANI–EB film with 15 wt % NMP under heating rate of 10°C/min is shown in Figure 8(a). According to this cure, there are three major stages of weight loss. The first weight loss is seen in the range of 298–358 K, which is because of the absorption of water molecules in the PANI–EB film during the dip-coating process.[37] The second weight loss is shown in the range of 358–388 K, which is specified to the weight loss of free NMP and probability to some water/NMP azeotrope. The NMP (b.p. 475–477 K at 760 mmHg) could not be completely removed from the films at the temperature range of 358–400 K because of residual NMP bound to the PANI backbone as evidenced by the second drop of TGA curve. Based on this, the third weight loss because of the removal of free NMP and lower oligomers of PANI occurs in the temperature range from 400 to 568 K, and the material loses about 60% of the original weight rapidly. The TGA curves showed that the weight loss of PANI–EB film varied from 21.5% (10 min) to 62.1% (30 min) for the 398 K regime. Further increase in the drying temperature ($T > 700$ K) might lead to the removal of bound NMP solvent. As a result, physical and chemical crosslinking reactions occur in PANI–EB structure. The thermogravimetric curve that corresponded to the precipitated form of PANI–EB (without residual NMP) is heated at a

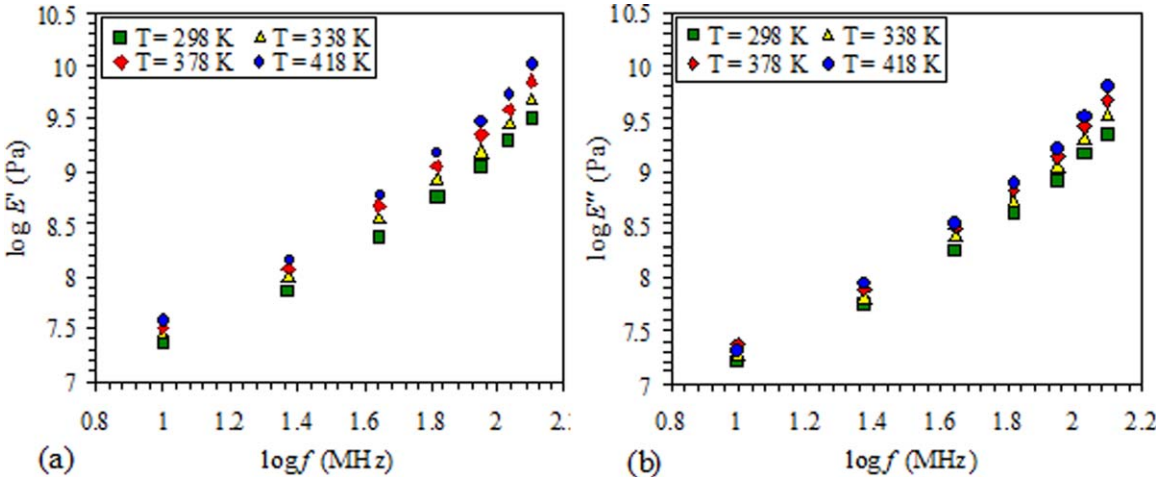


**Figure 5.** Log–log scale plots of $E'$ (a) and $E''$ (b) as functions of frequency, $f$, at different temperatures for PANI–EB film. [Color figure can be viewed in the online issue, which is available at wileyonlinelibrary.com.]

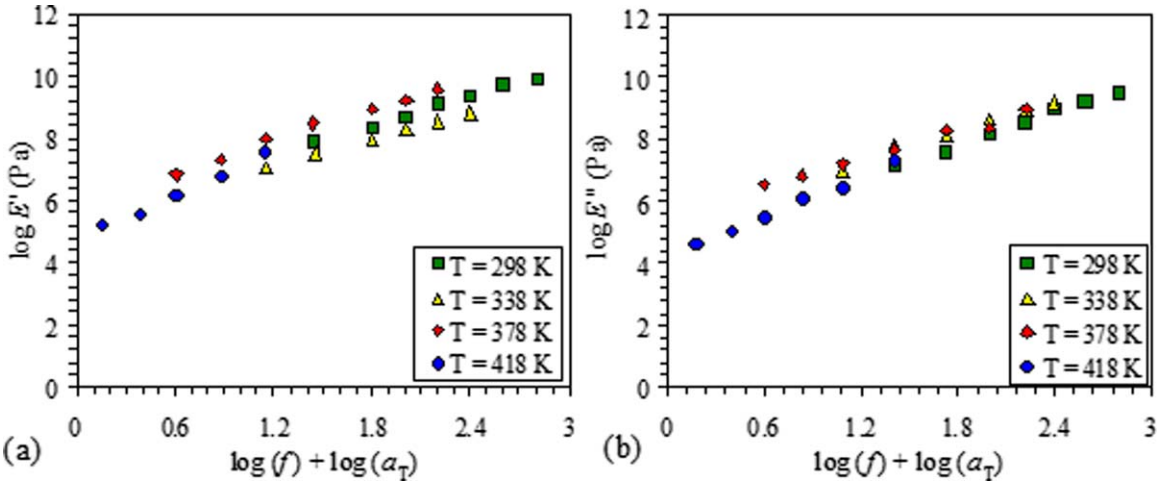


**Figure 6.** Master curve logarithmic plots for $E'$ (a) and log $E''$ (b) as functions of frequency, $f$, subject to shift factor values ($\alpha_T$) for PANI–EB films at different temperatures. [Color figure can be viewed in the online issue, which is available at wileyonlinelibrary.com.]

rate of 10°C/min as shown in Figure 8(b). The powder form of PANI–EB has one major weight loss, which was started from about 430 K up to temperatures more than 510 K. After this temperature range, the weight loss of film follows fairly linear behavior. In this stage, there is a minor weight loss (about 2%) in the range of 510–698 K. Further increase in the drying temperature ($T > 700$ K) might lead to the thermal degradation of PANI–EB structure, which has not been addressed in this study.

The variations of the shear modulus components ($E'$ and $E''$) with the weight loss percent of PANI–EB film under heating rate of 10°C/min are shown in Figure 9. It can be seen that the shear modulus components increase with the increase of the weight loss percent of the PANI–EB film. The outcome is a roughly linear correlation between shear modulus components and change in the weight loss.

**Role of Drying Time.** The variations of the $E'$ and $E''$ with drying time for the PANI–EB film dried at 378 K regime at a heating rate of 10°C/min are shown in Figure 10(a,b), respectively. The film thickness was determined to be 460 ± 15 nm. As shown in Figure 10(a), a sharp drop at around 379 K represents the $T_g$ is in good agreement with the experimental values reported in the literature.[37] DMTA results show that with increase of drying time, the $E'$ of the PANI–EB films increased significantly. For example, as can be seen from Figure 10(a), for the PANI–EB film heated at 348 K regime with increase of drying time from 10 min to 3 h, the $E'$ of the PANI–EB films increased from 2013 to 2792 MPa, respectively. In the extensively dried films that were prepared under vacuum for 24 h at 378 K, the value of $E'$ decreases significantly. The decrease of $E'$ would be connected with the increase of disordering of the PANI–EB structure because of the release of the NMP and the formation of some minor cracks at long-time drying. In addition, an increase of $T_g$ on long-time drying (24 h) was clearly shown based on these data. The abrupt decrease in $E'$ above $T_g$ is attributed to the release of free NMP solvent during heating process, where the second weight loss of PANI–EB film is observed [Figure 8(a)].

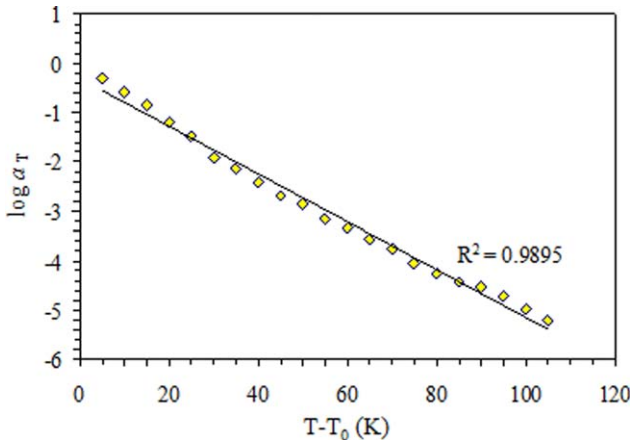


**Figure 7.** The variation of shift factor log $\alpha_T$ as a function of $T - T_0$ for PANI–EB films obtained by Arrhenius equation at temperatures ranging from 298 to 418 K. $T_0 = 293$ K. [Color figure can be viewed in the online issue, which is available at wileyonlinelibrary.com.]

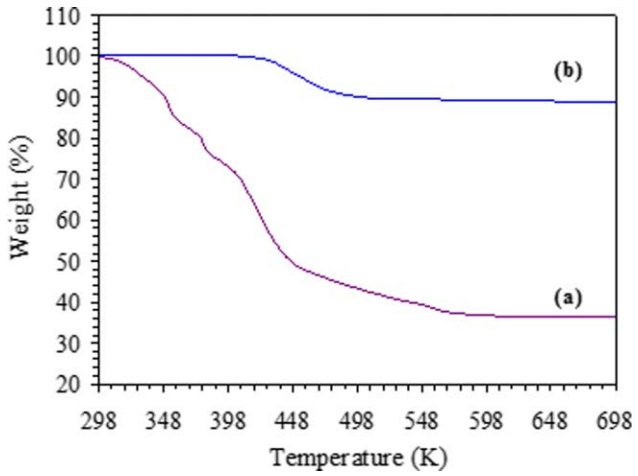


**Figure 8.** Thermogravimetric analysis of the PANI–EB film under heating rate of 10°C/min (a) as precipitated form (without residual NMP) and (b) film with 15 wt % of NMP solvent. [Color figure can be viewed in the online issue, which is available at wileyonlinelibrary.com.]

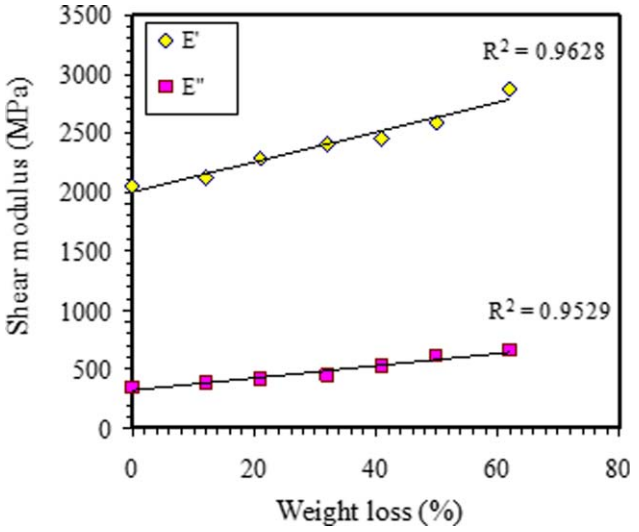


**Figure 9.** Variations of the shear modulus components with the weight loss percent of PANI–EB film under heating rate of 10°C/min. [Color figure can be viewed in the online issue, which is available at wileyonlinelibrary.com.]

There are two major three peaks in Figure 8(b). The first peak in the 313–324 K region is caused by the evaporation of water molecules and free NMP solvent in the PANI–EB film. This could be explained by the fact that the release of water molecules would provide more available active sites for NMP solvation, resulting in higher degree of NMP solvation level and change in the film stiffness and as a result $E'$ of PANI–EB film. The second peak in the 380–390 K regions is because of the evaporation of NMP molecules, assigned to the beginning of some crosslinking reactions. It can be seen from Figure 10(a) that the increase of $E'$ with drying time are related to the residual amount of water/NMP azeotrope in the PANI-EB film.

## Computational Simulations

The main aim of this section is to present a MD simulation study of the dynamical properties of PANI structure in the thermodynamic equilibrium state. In addition, the frequency range used in the experimental section implies that the relaxation time is on the order of 5–10 ns. This suggests that all the simulations generate equilibrium outcomes. The results are discussed in the following sections.

**Time Autocorrelation Function.** The result of TACF for PANI structure consisting of 40 aniline monomeric units at $T = 348$ K and $P = 1$ atm obtained from MD simulation and KWW equation is shown in Figure 11. The dotted solid line shows the reconstructed curve based on the KWW model [eq. (8)], and the dashed line shows the MD simulation runs. According to this figure, the following points should be mentioned: (1) all curves follow the similar exponential decay of TACF with timescale; however, the local conformational relaxation of PANI chains represented by MD simulation is fairly faster when compared with that obtained from KWW law. (2) The results show that in the long-time ($t >> \tau_1$) region, the trend of normal mode TACF curves are similar to each other. (3) The values of $\beta$ obtained by KWW model and MD simulation are 0.79 and 0.88, respectively. It suggests that the values of the stretching exponents obtained by KWW law provide the acceptable fit to the simulation data. These results are in good agreement with the data reported for pure polymer melt in the literature.[64]

**Fractional Free Volume.** Previous works have shown that when PANI–EB film is heated up, the free volume of the PANI chain increases, and the ability of the chain units to move in various directions also increases. When the free volume fraction attainable to the movement of atoms is small ($T < T_g$), polymer chain units can stretch or rotate around their axes without changes in the bond angle, whereas if the free volume fraction is largely increased ($T > T_g$), the chain units can freely slip past each other.[37,65] This increased mobility in either side chains or small groups of adjacent backbone atoms results in various transitions affecting thermal and viscoelastic properties of the polymer, notably a lowering of the $T_g$ and Young's modulus of the polymer.[34,65]

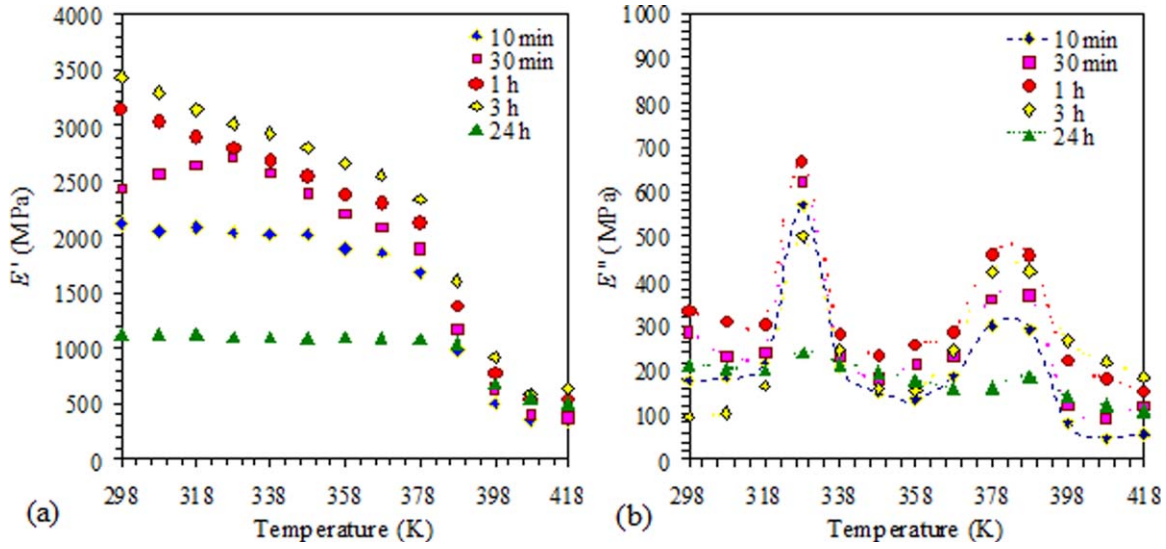


**Figure 10.** Variations of the $E'$ (a) and $E''$ (b) as functions of temperature for the PANI–EB film dried at 378 K at a heating rate of 10°C/min with different drying time. [Color figure can be viewed in the online issue, which is available at wileyonlinelibrary.com.]

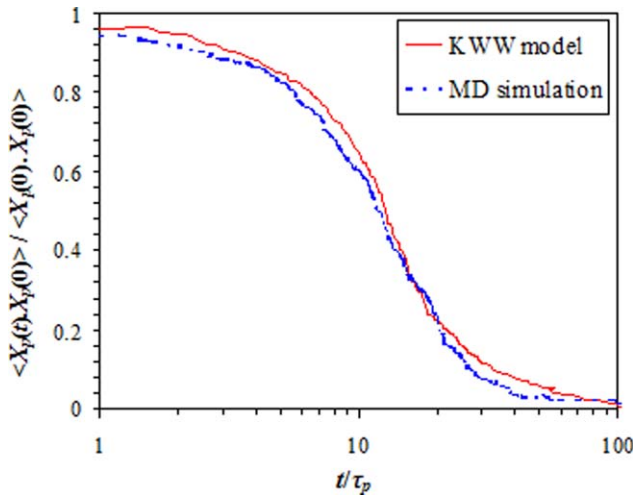


**Figure 11.** TACF for PANI structure. The solid line represents the curve obtained from the KWW model [eq. (6)], and the dashed line represents the result of MD simulation. [Number of aniline monomeric chain $N = 40$, $T = 348$ K, $P = 1$ atm]. [Color figure can be viewed in the online issue, which is available at wileyonlinelibrary.com.]

The fractional free volume ($f_g$) is the most common method to quantitatively calculate free volume size. The $f_g$ is used to characterize the efficiency of chain packing and free space in a polymer matrix. Theoretically, the $f_g$ was determined from Bondi and van Krevelen (B-K) method based on the following equation:[65]

$$V_f = (V - V_0), \tag{10}$$

where $V_f$ is the free volume, $V$ is the specific volume calculated from density, and $V_0$ is the occupied volume of the polymer chains. The $V_0$ was determined from the van der Waals volume of PANI chain according to the following equation:

$$V_0 = 1.3 V_w \tag{11}$$

The $f_g$ is defined as the ratio of free volume to the measured specific volume.

$$f_g = \frac{V_f}{V} \tag{12}$$

Table II represent the results of $f_g$ (in %) of PANI–EB structure at different temperatures based on the B-K method and MD simulation. The relative errors of simulation results in comparison with the theoretical results are 2.2, 1.1, 1.0, and 2.5% for temperatures 298, 348, 378, and 428 K, respectively. Therefore, the MD results are in excellent agreement with the $f_g$ data obtained from the B-K theoretical method. Both these results confirmed that the reported $f_g$ values are large for the PANI generated at high temperature.

**Cavity Size Distribution.** The CSD provides a comprehensive insight into the effect of free volume fraction on the viscoelastic properties of the PANI–EB films. CESA algorithm was applied to each of the PANI–EB structures at equilibrium thermodynamic state for the determination of the CSD.[66]

Figure 12 represents the CSD results of PANI–EB films simulated at temperatures of 298 K [Figure 12(a)], 338 K [Figure 12(b)], 378 K [Figure 12(c)], and 418 K [Figure 12(d)], which are obtained from CESA. The MD results show that the average cavity size with the highest probability density of the PANI at regimes of 298 K [Figure 12(a)], 338 K [Figure 12(b)], 378 K [Figure 12(c)], and 418 K [Figure 12(d)] are 8.4, 9.1, 10.1, and 10.7 Å, respectively. As depicted in the above-mentioned figures, considerable fractions of cavities appeared in the range of 5.0–12.0 up to 8.0–12.0 Å when the temperature increased from 298 to 418 K, respectively. It can be expected that with an increase in the cavity sizes of the PANI structure, a decrease in the free volume fraction value is accompanied, suggesting coalescence of smaller cavities to form larger cavities. The distributions of the simulated PANI at high temperature [Figure 12(c)] are shifted toward larger cavity size relative to the structure generated at low temperature [Figure 12(a)].

**Activation Energy.** According to the kinetic theory of elasticity, the $E'$ in the rubbery region is related to the activation energy ($E_a$) of polymer during decomposition process according to the following equation:[67]

$$E' = ART \exp(E_a/RT), \tag{13}$$

where $X_c$ is crosslink density (mol/cm$^3$), $A$ is a constant, $R$ is the gas universal constant, $T$ is the absolute temperature, and $E_a$ is the activation energy for decomposition of PANI. The plot of $\ln E'/T$ versus $1000/T$ for the PANI film is shown in Figure 13. From the slope of the exponential fit, the $E_a$ for decomposition of the simulated PANI structure consists of 30, 40, and 50 aniline units, which correspond to 15.1 kJ/mol ($R^2 = 0.97$), 15.4 kJ/mol ($R^2 = 0.98$), and 15.8 kJ/mol ($R^2 = 0.98$), respectively. The current simulation results are close to the calculated value obtained from the Arrhenius model ($E_a = 20.3$ kJ/mol). In addition, this result is in the range of activation energy values reported in the literature ($E_a \approx 21.7$–$27.5$ kJ/mol)[32,48,62,63,65] based on the Coats and Redfern method.[68]

## CONCLUSIONS

Viscoelastic behavior of PANI–EB films with mean thickness of $460 \pm 15$ nm are investigated from two viewpoints of experimental work and MD simulations. Experiments were performed by PANI–EB film prepared chemically in two series of NMP-free and with 15 wt % NMP as a solvent. TEM images showed that crosslinked PANI films consist of high aspect ratio of nanofibers, having lengths up to 500 nm and diameters of about 20–80 nm. Viscoelastic properties of prepared films are studied using DMTA measurements and TGA analysis based on parameters including drying temperature, residual solvent content,

**Table II.** Fractional Free Volume ($f_g$, in %) of the PANI–EB Structure at Different Temperatures Based on the Bondi–van Krevlen Method[65] and MD Simulation

| | Temperature (K) | | | |
|---|---|---|---|---|
| $f_g$ (%) | 298 | 348 | 378 | 418 |
| Bondi–van Krevlen method | 0.403 | 0.481 | 0.512 | 0.596 |
| MD simulation | 0.394 | 0.476 | 0.507 | 0.581 |

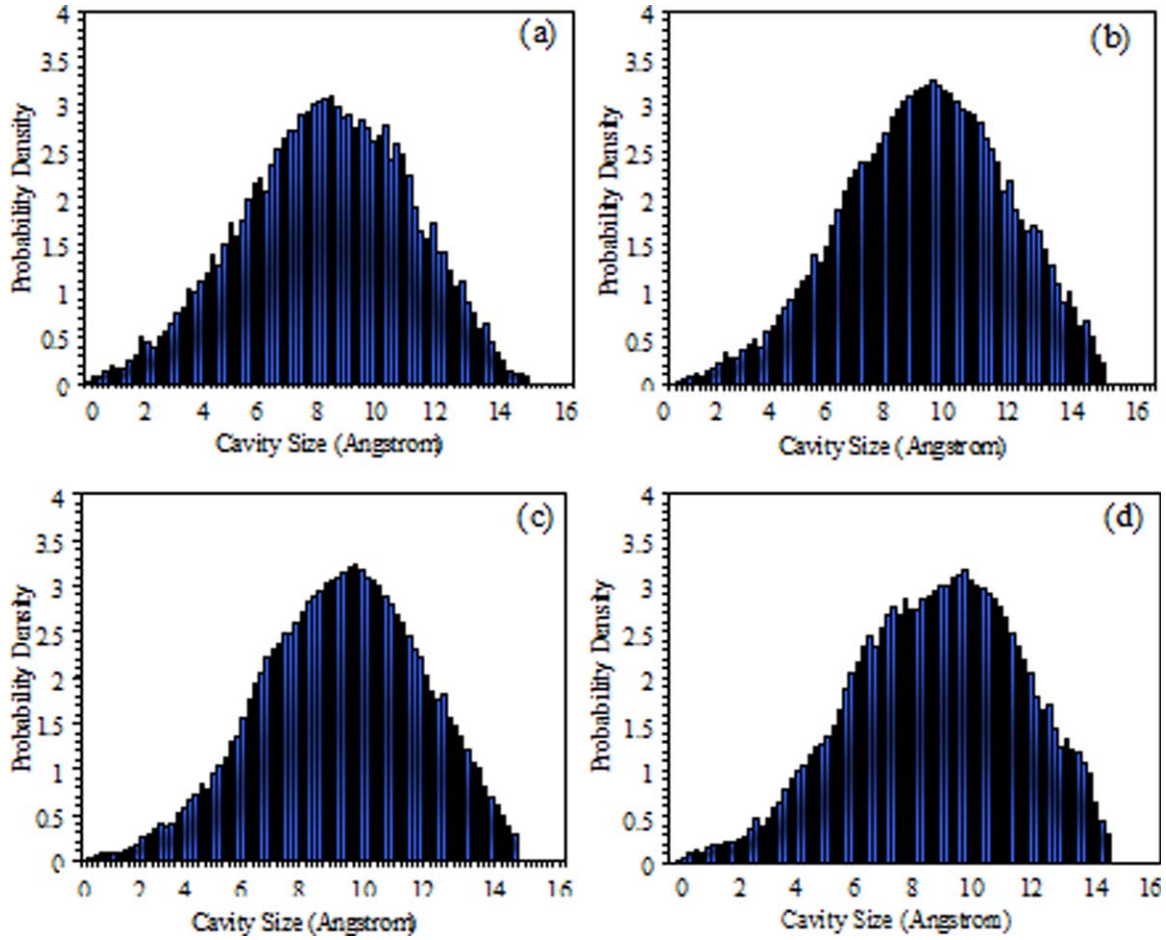


**Figure 12.** Cavity size distribution of simulated PANI film at temperatures of (a) 298 K, (b) 338 K, (c) 378 K, and (d) 418 K. [Color figure can be viewed in the online issue, which is available at wileyonlinelibrary.com.]

and drying time. From qualitative observation of the storage modulus $[E'(\omega,T)]$ and loss modulus $[E''(\omega,T)]$ data, the effects of drying temperature $T$ and drying time associated with the residual NMP were found to be dramatic and modest, respectively. The effect of temperature was variable based on the $T_g$ of PANI–EB film. At $T \leq 378$, where $T = 378$ K corresponds to $T_g$, $E'$ values are higher than those of $E'$ obtained at $T > 378$ K. However, the reduction trend of $E'$ with increasing of $T$ in both regions is similar. From quantitative standpoint, the $E'$ of PANI–EB film significantly decreased by three orders of magnitude from the values of about 5.5 ($\pm$ 0.2) GPa to 3.5 ($\pm$ 0.2) MPa in the temperature range of 350–410 K, which quantifies film softening. DMTA results show that with the increase of drying time, the $E'$ increased from 2013 to 2792 MPa, when drying time increased from 3 to 24 h, respectively. There is an approximately linear correlation between $E'$ and residual NMP, and the value of $E'$ increased from 2015 to 2874 MPa when the weight loss of film changed from 0 to 60%. DMTA measurements exhibited that the $E'$ decreased from 3143 to 2133 MPa, when the drying temperature increased from 298 to 378 K, respectively. Using the principle of time–temperature superimposition, a master curve was generated at a reference temperature by shifting isothermal curves with respect to an arbitrarily selected reference temperature on a logarithmic timescale. Experimentally determined shift factors enabled the determination of the activation energy associated with film relaxation processes, from the value of which crosslinking reactions between PANI chains was inferred. Based on the Arrhenius

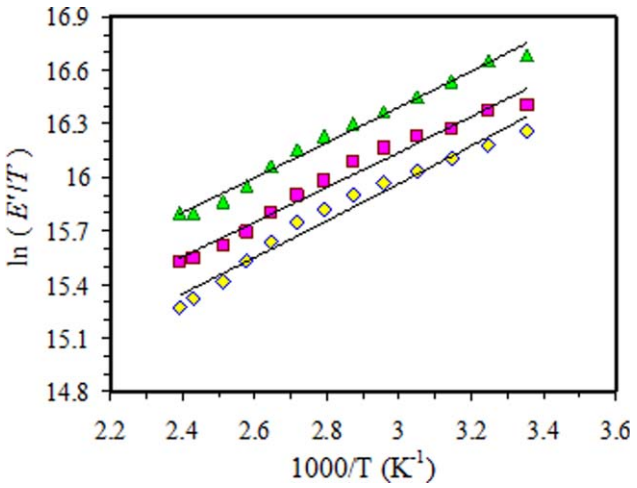


**Figure 13.** Plots of ln $(E'/T)$ as a function of temperature for the PANI. [Line was linearly fitted]. [Color figure can be viewed in the online issue, which is available at wileyonlinelibrary.com.]

model, the value of activation energy of PANI–EB structure was determined to be 20.3 kJ/mol.

Computationally, MD simulation is performed using COMPASS force field associated with energy minimization over the temperature ranges of 298–418 K associated with different monomeric aniline chains. The temperature dependence of viscoelastic properties can provide an adequate understanding of its effect on the free volume fraction, CSD, and activation energy of generated PANI structures. The $f_g$ and CSDs of the PANI were calculated using a CESA algorithm. Qualitatively, it was exhibited that both $f_g$ and CSD shifted toward larger value by increase of the simulation temperature. Finally, it was shown that the MD results provide a fairly good compatibility with the experimental data. It can be suggested that wider exploration of the viscoelastic behavior of PANI–EB nanostructured films will open a new insight and will assist rational design of devices constructed based on this polymer.

## ACKNOWLEDGMENTS

The authors thank the Hamedan University of Technology and Laser and Optic Research School of Iran for TGA analysis, DMTA measurements, optical experiments, and image processing analysis.

## REFERENCES

1. Yang, P.; Yang, W. *Chem. Rev.* **2013**, *113*, 5547.
2. Belaabed, B.; Lamouri, S.; Naar, N.; Bourson, P.; Hamady, S. O. S. *Polym. J.* **2010**, *42*, 546.
3. Sudha, J. D.; Ramakrishnan, R. *J. Appl. Polym. Sci.* **2013**, *128*, 1756.
4. Otto, S. W. *Anal. Chem.* **2002**, *74*, 2663.
5. Rangari, V. K.; Samsur, R.; Jeelani, S. *J. Appl. Polym. Sci.* **2013**, *129*, 1249.
6. Ucan, D.; Kanik, F. E.; Karatas, Y.; Toppare, L. *Sens. Actuators B: Chem.* **2014**, *201*, 545.
7. MacDiarmid, A. G.; Chiang, J. C.; Richter, A. F.; Epstein, A. J. *Synth. Met.* **1987**, *18*, 285.
8. Frau, A. F.; Lane, T. J.; Schlather, A. E.; Park, J. Y.; Advincula, R. C. *Ind. Eng. Chem. Res.* **2011**, *50*, 5532.
9. Lu, W.; Fadeev, A. G.; Qi, B. H.; Smela, E.; Mattes, B. R.; Ding, J.; Spinks, G. M.; Mazurkiewicz, J.; Zhou, D. Z.; Wallace, G. G.; MacFarlane, D. R.; Forsyth, S. A.; Forsyth, M. *Science* **2002**, *297*, 983.
10. Nathalie, K.; Guimard, N. G.; Schmidt, C. E. *Prog. Polym. Sci.* **2007**, *32*, 876.
11. Kim, C.; Facchetti, A.; Marks, T. J. *Science* **2007**, *318*, 76.
12. Wang, Y.; Acton, O.; Ting, G.; Weidner, T.; Shamberge, P. J.; Ma, H.; Ohuchi, F. S.; Castner, D. G.; Jen, A. K.-Y. *Org. Electron.* **2010**, *11*, 1066.
13. Yan, H.; Chen, Z.; Zheng, Y.; Newman, C.; Quinn, J. R.; Dötz, F.; Kastler, M.; Facchetti, A. *Nature* **2009**, *457*, 679.
14. Keddie, J. L.; Jones, R. A. L.; Cory, R. A. *Faraday Discuss.* **1994**, *98*, 219.
15. Keddie, J. L.; Jones, R. A. L.; Cory, R. A. *Europhys. Lett.* **1994**, *27*, 59.
16. Pei, H.; Hong, L.; Lee, J. Y. *J. Membr. Sci.* **2008**, *307*, 126.
17. Shinde, S. D.; Jayakannan, M. *J. Appl. Polym. Sci.* **2013**, *127*, 1781.
18. Madathil, R.; Parkesh, R.; Ponrathnam, S.; Large, M. C. J. *Macromolecules* **2004**, *37*, 2002.
19. Rebouillat, S.; Pla, F. *J. Biomater. Nanobiotechnol.* **2013**, *4*, 165.
20. Antony, M. J.; Jayakannan, M. *Langmuir* **2011**, *27*, 6268.
21. Conklin, J. A.; Huang, S.-C.; Huang, S.-M.; Wen, T.; Kaner, R. B. *Macromolecules* **1995**, *28*, 6522.
22. Wei, Y.; Jang, G. W.; Hsueh, K. F.; Scherr, E. M.; MacDiarmid, A. G.; Epstein, A. J. *Polymer* **1992**, *33*, 314.
23. Sreedhar, B.; Sairam, M.; Chattopadhyay, D. K.; Paromita Mitra, P.; Mohan Rao, D. V. *J. Appl. Polym. Sci.* **2006**, *101*, 499.
24. Zheng, W.; Min, Y.; MacDiarmid, A. G.; Angelopoulos, M.; Liao, Y.-H.; Epstein, A. J. *Synth. Met.* **1997**, *84*, 63.
25. Anitha, G.; Subramanian, E. *Sens. Actuators B: Chem.* **2003**, *92*, 49.
26. Stejskal, J.; Sapurina, I.; Trchová, M. *Prog. Polym. Sci.* **2010**, *35*, 1420.
27. Garai, A.; Shreyam, C.; Nandi, A. K. *Synth. Met.* **2010**, *160*, 1733.
28. Lambooy, P.; Phelan, K. C.; Haugg, O.; Krausch, G. *Phys. Rev. Lett.* **1996**, *76*, 1110.
29. O'Connell, P. A.; McKenna, G. B. *Rev. Sci. Instrum.* **2007**, *78*, 01390101.
30. Wu, X.-F.; Dzenis, Y. A. *J. Phys. D: Appl. Phys.* **2005**, *38*, 2848.
31. Han, M. G.; Lee, Y. J.; Byun, S. W.; Im, S. S. *Synth. Met.* **2001**, *124*, 337.
32. Rodrigues, P. C.; de Souza, G. P.; Da Motta Neto, J. D.; Akcelrud, L. *Polymer* **2002**, *43*, 5493.
33. Lurio, L.; Kim, H.; Ruhm, A.; Basu, J.; La, J.; Sinha, S.; Mochrie, S. G. J. *Macromolecules* **2003**, *36*, 5704.
34. Hillman, A. R.; Mohamoud, M. A.; Efimov, I. *Anal. Chem.* **2011**, *83*, 5696.
35. Jasna, V.; Džunuzović, M. V.; Pergal, R. P.; Ostojić, S.; Lazić, N.; Špírková, M.; Jovanović, S. *Ind. Eng. Chem. Res.* **2012**, *51*, 10824.
36. Prathab, B.; Aminabhavi, T. B. *J. Appl. Polym. Sci.* **2007**, *45*, 1260.
37. Bahramian, A. *Appl. Surf. Sci.* **2014**, *311*, 508.
38. Sasani Ghamsaria, M.; Bahramian, A. *Mater. Lett.* **2008**, *62*, 361.
39. Fischer, F.; Charlotte, F. *Comput. Phys. Commun.* **1987**, *43*, 355.
40. Theodorou, D. N.; Suter, U. W. *Macromolecules* **1985**, *18*, 1467.
41. Sun, H. *J. Phys. Chem. B* **1998**, *102*, 7338.
42. Varela-Álvarez, J. A.; Sordo, A.; Scuseria, G. E. *J. Am. Chem. Soc.* **2005**, *127*, 11318.

43. Peathab, B.; Aminabhavi, T. M. *J. Polym. Sci. Part B: Polym. Phys.* **2007**, *45*, 1260.
44. Svärd, M.; Rasmuson, Å. C. *Ind. Eng. Chem. Res.* **2009**, *48*, 2899.
45. Yamamoto, T. *Polymer* **2009**, *50*, 1975.
46. Ostwal, M. M.; Pellegrino, J. J.; Norris, I. D.; Tsotsis, T. T.; Sahimi, M.; Mattes, B. R. *Ind. Eng. Chem. Res.* **2005**, *44*, 7860.
47. Leonarski, F.; Trovato, F.; Tozzini, V.; Leś, A.; Trylska, J. *J. Chem. Theory Comput.* **2013**, *9*, 4874.
48. Ferry, J. D. Viscoelastic Properties of Polymers; Wiley: New York, **1980**.
49. Maron, J.; Winokur, M. J.; Mattes, B. R. *Macromolecules* **1995**, *28*, 4475.
50. Stejskal, J.; Gilbert, R. G. *Pure Appl. Chem.* **2002**, *74*, 857.
51. Nosé, S. *J. Chem. Phys.* **1984**, *81*, 511.
52. Hoover, W. G. *Phys. Rev. A* **1985**, *31*, 1695.
53. Kadam, V.; Nicolai, T.; Nicol, E.; Benyahia, L. *Macromolecules* **2011**, *44*, 8225.
54. Matsumiya, Y.; Uno, A.; Watanabe, H.; Inoue, T.; Urakawa, O. *Macromolecules* **2011**, *44*, 4355.
55. Grant, D. S.; Smith, D.; Borodin, O. *J. Chem. Phys.* **2002**, *117*, 10350.
56. Rouse, P. E. *J. Chem. Phys.* **1953**, *21*, 1272.
57. Holm, C.; Kremer, K. Advanced Computer Simulation Approaches for Soft Matter Sciences; Springer: Berlin Heidelberg, **2005**; Vol. 2.
58. Bendler, J. T.; Shlesinger, M. F. *Macromolecules* **1985**, *18*, 591.
59. William, M. L.; Landel, R. F.; Ferry, J. D. *J. Am. Chem. Soc.* **1955**, *77*, 3701.
60. Macosko, C. W. Rheology: Principles, Measurements and Applications; Wiley-VCH: New York, **1994**; pp. 175–378.
61. Sohn, I.-S.; Park, C.-W. *Ind. Eng. Chem. Res.* **2002**, *41*, 2418.
62. Tsai, T.-C.; Tree, D. A.; High, M. S. *Ind. Eng. Chem. Res.* **1994**, *33*, 2600.
63. von Meerwall, E.; Beckman, S.; Jang, J.; Mattice, W. L. *J. Chem. Phys.* **1998**, *108*, 4299.
64. Riande, E.; Diaz Calleja, E.; Prolongo, M. G.; Masegosa, R. M.; Salom, C. Polymer Viscoelasticity; Marcel Dekker: New York, **2000**.
65. van Krevelen, D. W. Properties of Polymers, 3rd ed.; Elsevier Science: Amsterdam, **1990**.
66. Wang, X.-Y.; Raharjo, R. D.; Lee, H. J.; Lu, Y.; Freeman, B. D.; Sanchez, I. C. *J. Phys. Chem. B* **2006**, *110*, 12666.
67. Pan, H.; Chen, D. *Eur. Polym. J.* **2007**, *43*, 3766.
68. Coats, A. W.; Redfern, J. P. *Nature* **1964**, *201*, 68.